ACS Chemical Neuroscience

pubs.acs.org/chemneuro
Letter

Increased Cerebral Level of P2X7R in a Tauopathy Mouse Model by PET Using [^{18}F]GSK1482160

Published as part of the ACS Chemical Neuroscience special issue "Monitoring Molecules in Neuroscience 2023".

Yanyan Kong, Lei Cao, Jiao Wang, Junyi Zhuang, Yongshan Liu, Lei Bi, Yifan Qiu, Yuyi Hou, Qi Huang, Fang Xie, Yunhao Yang, Kuangyu Shi, Axel Rominger, Yihui Guan, Hongjun Jin,* and Ruiqing Ni*

Cite This: *ACS Chem. Neurosci.* 2024, 15, 2112–2120

Read Online

ACCESS | Metrics & More | Article Recommendations | Supporting Information

ABSTRACT: Neuroinflammation plays an important role in Alzheimer's disease and primary tauopathies. The aim of the current study was to map [^{18}F]GSK1482160 for imaging of purinergic P2X7R in Alzheimer's disease and primary tauopathy mouse models. Small animal PET was performed using [^{18}F]-GSK1482160 in widely used mouse models of Alzheimer's disease (APP/PS1, 5×FAD, and 3×Tg), 4-repeat tauopathy (rTg4510) mice, and age-matched wild-type mice. Increased uptake of [^{18}F]GSK1482160 was observed in the brains of 7-month-old rTg4510 mice compared to wild-type mice and compared to 3-month-old rTg4510 mice. A positive correlation between hippocampal tau [^{18}F]APN-1607 and [^{18}F]GSK1482160 uptake was found in rTg4510 mice. No significant differences in the uptake of [^{18}F]GSK1482160 was observed for APP/PS1 mice, 5×FAD mice, or 3×Tg mice. Immunofluorescence staining further indicated the distribution of P2X7Rs in the brains of 7-month-old rTg4510 mice with accumulation of tau inclusion. These findings provide in vivo imaging evidence for an increased level of P2X7R in the brains of tauopathy mice.

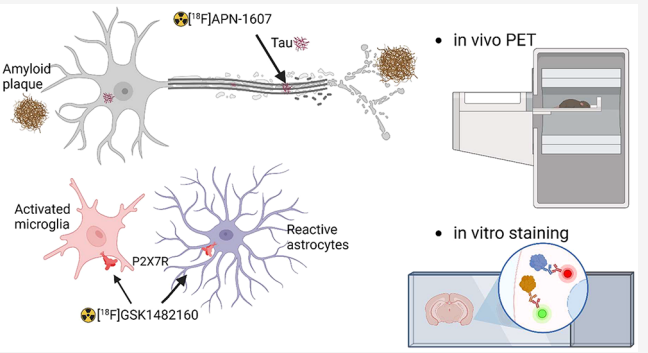

KEYWORDS: *Alzheimer's disease, amyloid-β, glia, P2X7R, PET, tau*

INTRODUCTION

Alzheimer's disease (AD) is the most common cause of dementia and is pathologically characterized by amyloid-β (Aβ) plaque and tau tangle deposition. Primary tauopathies such as frontotemporal lobar degeneration (FTLD), corticobasal degeneration (CBD), and progressive supranuclear palsy (PSP) are pathologically characterized by tau inclusions. Neuroinflammation plays an important role in AD and primary tauopathies. Purinergic signaling is important for cognitive disturbances, cognitive impairment, and neuropsychiatric symptoms of AD.[1] Purinergic receptors, particularly P2X7Rs, play important roles in chronic immune and inflammatory responses.[1] In the central nervous system, P2X7R is expressed on microglia, astrocytes[2] and oligodendrocytes, but its expression on neurons is still unclear.[1] P2X7R has proinflammatory functions by increasing the level of adenosine triphosphate, which activates P2X7R and leads to proinflammatory cytokines. Increased expression and activation of P2X7Rs have been reported in post-mortem brains from patients with AD, FTLD, or PSP.[3] In addition, P2X7Rs are involved in important pathological processes in the development of AD, including Aβ production and plaque formation, tau tangles, oxidative stress, and chronic neuroinflammation. There is a vicious cycle between Aβ and alterations in the levels of P2X7Rs: P2X7Rs promote proinflammatory pathways via Aβ-mediated chemokine release,[4] particularly through the chemokine CCL3, which is associated with pathogenic CD8+ T-cell recruitment.[4] In addition, P2X7R affects Aβ production by influencing α-secretase-dependent amyloid precursor protein processing[5] and increasing plaque formation mediated by glycogen synthase kinase-3β.[6] P2X7R also influences the aggregate burden of tau in human tauopathies and results in distinct signaling in microglia and astrocytes.[7] Upregulated expression levels of P2X7Rs in AD mouse models have been reported, such as in rats injected with $A\beta_{42}$,[8] APP/PS1 mice,[4] J20 mice,[9] and tauopathy THY-Tau22 mice;[3] moreover, deficiency of the *p2rx7* gene or pharmacological inhibition of P2RX7 has been shown to improve plasticity and cognitive ability in P301S tau transgenic mice[10] and amyloidosis mice.[4]

Received: January 29, 2024
Revised: May 16, 2024
Accepted: May 17, 2024
Published: May 22, 2024

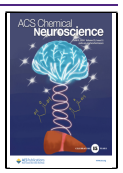

https://doi.org/10.1021/acschemneuro.4c00067
ACS Chem. Neurosci. 2024, 15, 2112–2120

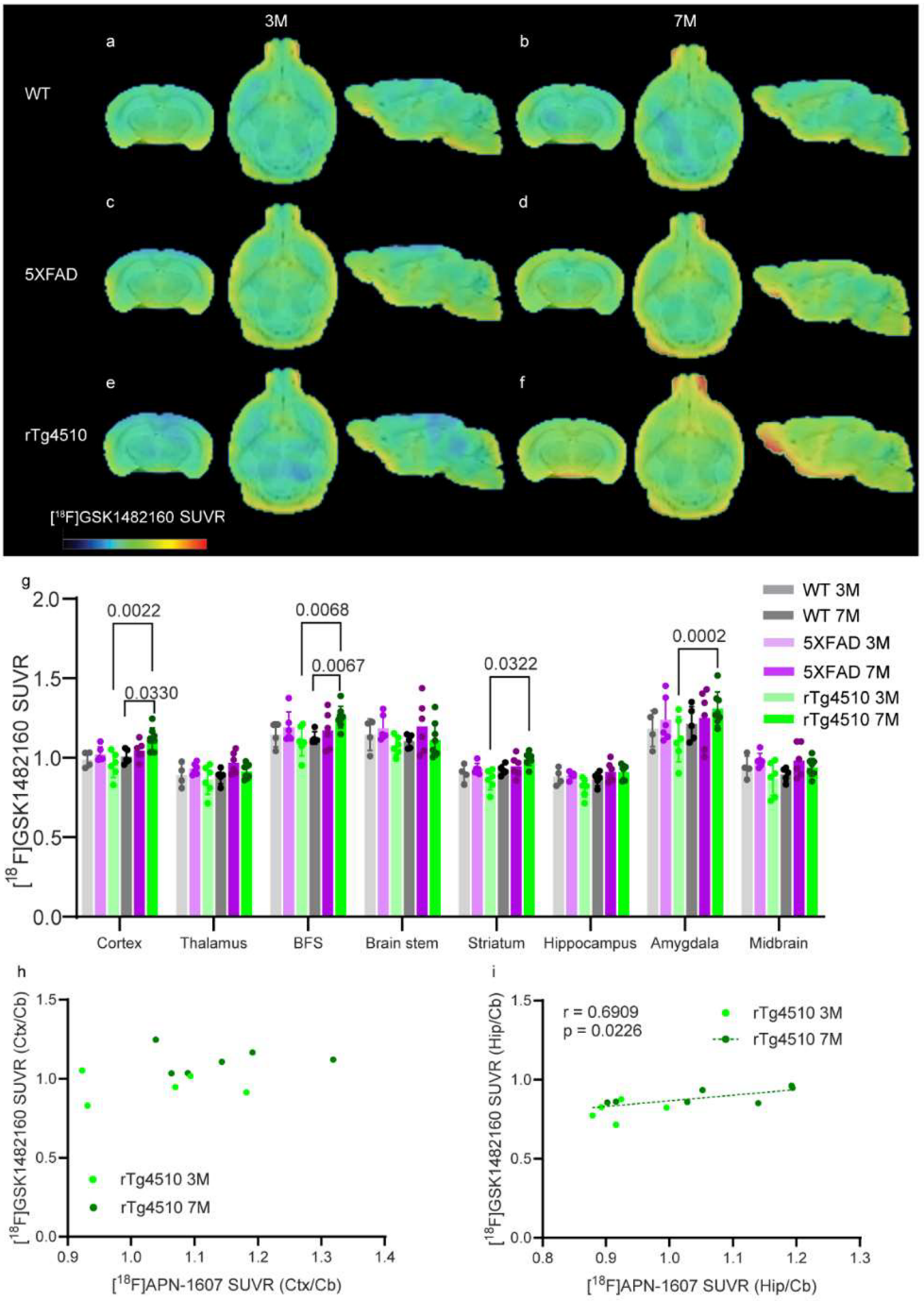

Figure 1. Increased regional [^{18}F]GSK-1482160 brain uptake in 7-month-old rTg4510 mice compared to age-matched wild-type mice and correlation with [^{18}F]APN-1607 uptake in the brain. (a−f) Representative [^{18}F]GSK-1482160 SUVR images of 3- and 7-month-old WT (a, b), 5×FAD (c, d), and rTg4510 (e, f) mice; SUVR scale, 0−2.2. BFS, basal forebrain system. (g) Quantification of [^{18}F]GSK-1482160 SUVRs in WT, 5×FAD, and rTg4510 mice. (h, i) Nonparametric Spearman's rank analysis of [^{18}F]GSK-1482160 and [^{18}F]APN-1607 SUVR (Cb as the reference region) in rTg4510 mice (3 months, n = 5; 7 months, n = 6). HIP, hippocampus. Ctx, cortex. Cb, cerebellum.

Pharmacological or genetic P2X7R blockage reversed the proteasomal impairment induced by P301S tau in mice.[11] Thus, P2X7R is a promising target for neuroinflammation imaging and is a therapeutic target for AD and primary tauopathies.

Several positron emission tomography (PET) tracers for P2X7R have been developed,[12] including [^{18}F]JNJ-64413739[13] (K_d = 1.0 nM), [^{18}F]GSK1482160 (K_d = 4.3 nM),[14] [^{11}C]SWM139[15] (K_d = 4.6 nM), [^{18}F]IUR-1601[16] (K_i = 4.3 nM) [^{11}C]A-740003[17] (K_i = 0.1 nM), [^{123}I]TZ6019[18] (K_i = 6.3 nM), [^{18}F]PTTP[19] (K_d = 12.4 nM), and [^{18}F]FTTM[20] (K_d = 25.4 nM) (the affinities are measured on hP2X7R). Earlier study showed that [^{11}C]SMW139 showed a 6 times lower affinity for the rodent P2X7R than the human P2X7R and was rapidly metabolized in mice, with 30+% unmetabolized plasma fraction.[15,21] Increased [^{18}F]JNJ-64413739 uptake was reported in the brain and peripheral organs of animal models of epilepsy[22] and lipopolysaccharide (LPS)-injected mice.[23]

https://doi.org/10.1021/acschemneuro.4c00067
ACS Chem. Neurosci. 2024, 15, 2112−2120

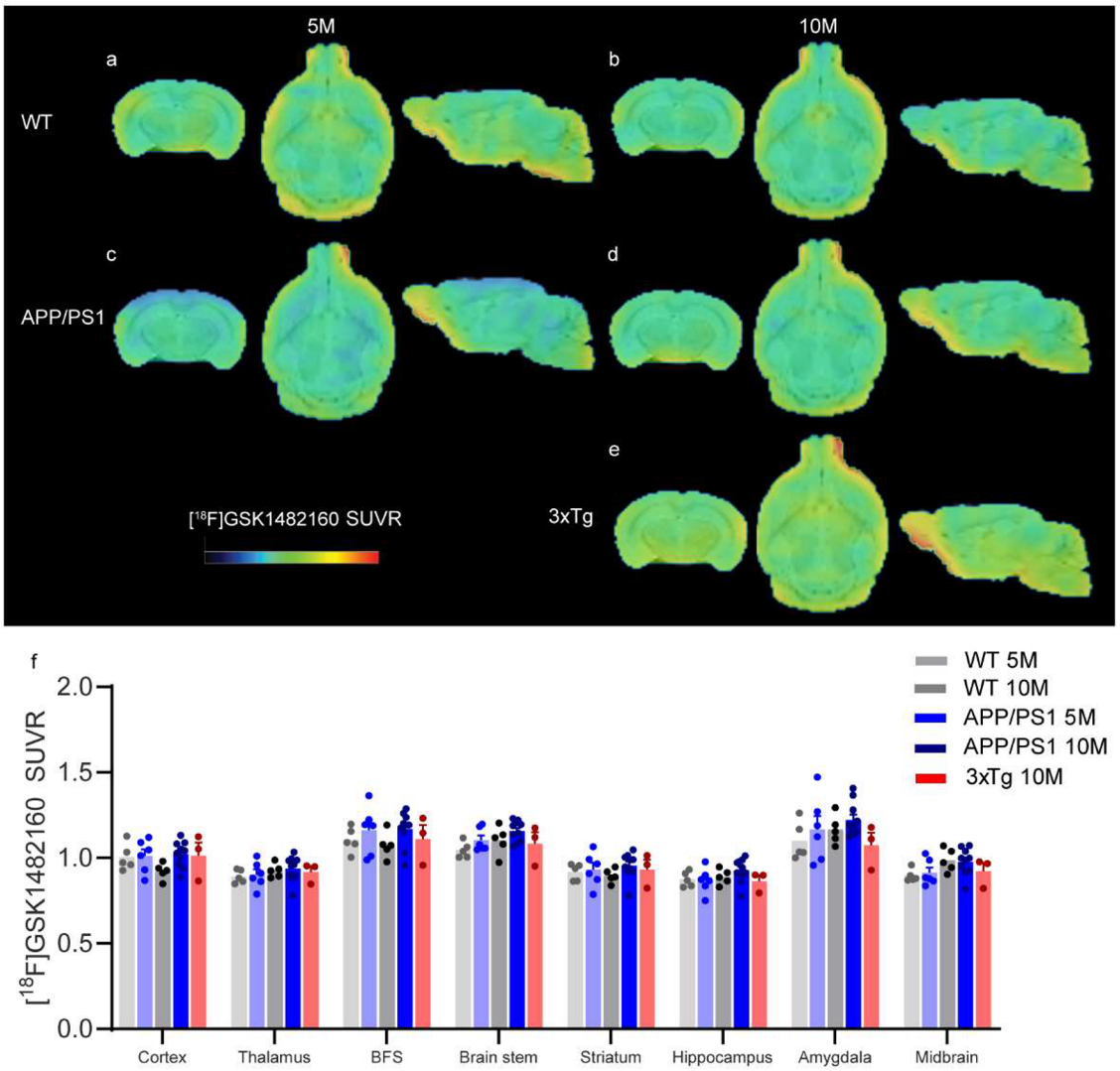

Figure 2. No difference in regional [^{18}F]GSK-1482160 cerebral uptake between 5- or 10-month-old APP/PS1 mice or 3×Tg mice and wt mice. (a–e) Representative [^{18}F]GSK-1482160 SUVR images in the brain of 5- and 10-month-old WT (a, b), APP/PS1 (c, d), and 10-month-old 3×Tg (e) mice; SUVR scale 0–2.2; BFS, basal forebrain system. (f) Quantification of [^{18}F]GSK-1482160 SUVRs in the brain of WT, APP/PS1 mice, and 3×Tg mice.

Increased uptake of [^{11}C]GSK1482160 has also been reported in the cortex and hippocampus of LPS-treated mice in a blockable manner.[24] Here we chose [^{18}F]GSK1482160 for its affinity in the rodent, suitable pharmacokinetics, and metabolic stability based on previous detailed characterization study[25] and for its availability. To date, the in vivo pattern of P2X7R in AD models and in tauopathy models has not been elucidated, with two studies reporting on a 12- to 13-month-old APP/PS1 mouse model using [^{18}F]4A.[26] and 5- to 14-month-old APP/PS1-21 mice using [^{11}C]SMW139 (no difference in cerebral uptake compared to wild-type mice).[21] An earlier autoradiography study using [^{11}C]SMW139 showed comparable binding in temporal cortex tissue from AD patients and controls,[15]

The aim of the current study was to evaluate changes in the levels of P2X7R by using [^{18}F]GSK1482160 PET in widely used transgenic mouse models in AD research. The use of different animal models facilitates the understanding of the contribution of amyloid and tau to P2X7R alterations in the brain. The amyloidosis models APP/PS1[27] and 5×FAD mice[28] develop cerebral amyloid plaque deposits in the cortical and subcortical regions, with abundant deposits seen in APP/PS1 at 9 months and at a younger age (4–5 months) in 5×FAD mice.[29] In comparison 3×Tg mice develop both amyloid and tau deposits in the brain; however, at around 10 months, only mild accumulation mainly in the subiculum was detected in this strain due to genetic drift.[30,31] rTg4510 (P301L) tau mice[32] is one of the most widely used model of 4-repeat tauopathy, with abundant tau pathology at 7 months in the cortical regions, hippocampus, and gliosis.[33] Recent study showed a 4-fold upregulation in the *p2rx7* level in the brain of rTg4510 mice at 6 months compared to wild-type mice.[7] We assessed the alterations of regional P2X7R levels in response to the amyloid and/or tau accumulation in APP/PS1 mice (5 months, 10 months), 3×Tg mice (10 months), 5×FAD mice (3 and 7 months), rTg4510 mice (3 and 7 months), and age-matched wild-type mice. Ex vivo staining was performed to determine the distribution of P2X7R in the brain of the mice that underwent in vivo imaging.

https://doi.org/10.1021/acschemneuro.4c00067
ACS Chem. Neurosci. 2024, 15, 2112–2120

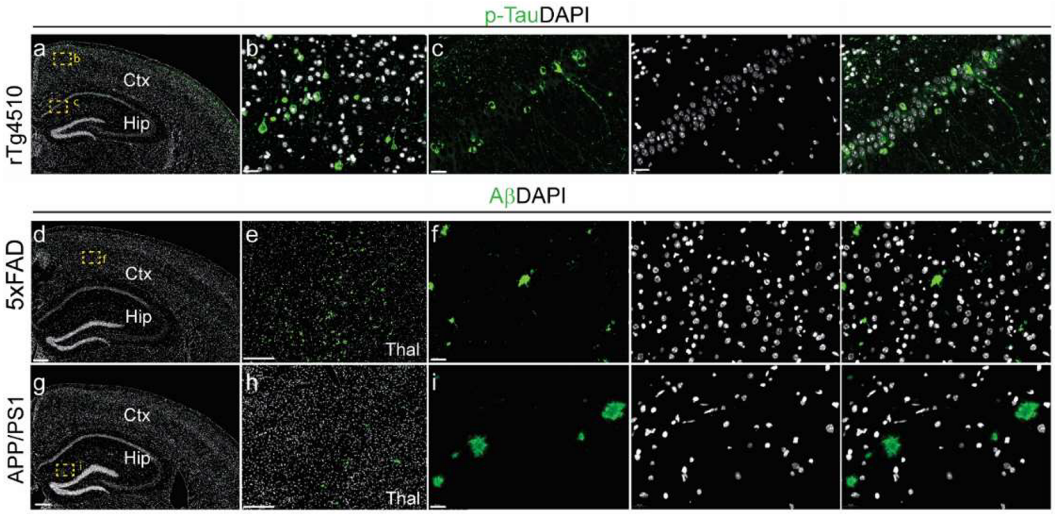

Figure 3. Staining of tau inclusions in the brain from 7-month-old rTg4510 mice and amyloid-β deposits in the brains of 7-month-old 5×FAD mice and 10-month-old APP/PS1 mice. (a−c) An overview and zoomed-in view of the staining of phospho-Tau (p-Tau, green) in coronal brain slices from 7-month-old rTg4510 mice. (c) Zoomed-in view showed tau tangles in the cortex (Ctx), and hippocampus (Hip). (d−i) Overviews and a zoomed-in view of the staining of coronal brain slices from 7-month-old 5×FAD mice and 10-month-old APP/PS1 mice. Zoomed-in views revealing the presence of amyloid-β deposits (green) in the cortex (Ctx) of 5×FAD mice (e, f) and hippocampus (Hip) of 10-month-old APP/PS1 mice (h, i). The yellow squares in the overviews indicate the locations of the zoom-ins. The nuclei were counterstained with DAPI (white). Scale bar = 200 μm (a, d, e, g, h) or 20 μm (b, c, f, i). Thal, thalamus.

RESULTS AND DISCUSSION

The Regional Uptake of [^{18}F]GSK1482160 Was Greater in rTg4510 Mice than in Age-Matched Wild-Type Mice and Correlated with Tau Deposits in the Hippocampus. The high-performance liquid chromatography (HPLC) and quality control results for [^{18}F]GSK1482160 are shown in Figure S1. The dynamics of [^{18}F]GSK1482160 in the periphery of mouse and rat models and the in vitro and in vivo stabilities of [^{18}F]GSK1482160 were demonstrated in a recent study.[25] We found that [^{18}F]GSK1482160 exhibited relatively lower uptake inside the mouse brain than outside the mouse brain (Figure S2). The uptake of [^{18}F]GSK1482160 in the brain was relatively low around 0.7 in the wild-type mice (Figures S2 and S3). In contrast to translocator protein (TSPO) imaging, which is known to show a high cerebellar uptake,[33,34] we found that the cerebellar uptake of [^{18}F]-GSK1482160 in the mouse brain was not much greater than that of cerebral regions (Figure S3). In an earlier P2X7R imaging study using [^{18}F]JNJ-64413739 in a rodent model, the cerebellum was also used as the reference region for SUVR calculations.[23] The cerebellum is suitable for use as a reference brain region for [^{18}F]GSK1482160. rTg4510 mice are known to develop tau pathology at approximately 5 months of age.[32] To determine whether and when alterations in the levels of P2X7R in the brain of the rTg4510 tau mouse model are related to tau accumulation, we assessed [^{18}F]GSK1482160 imaging in 3- and 7-month-old (with tau pathology) rTg4510 mice. We quantified the regional [^{18}F]GSK1482160 relative standardized uptake value (SUVR) using the cerebellum as the reference region. We observed that the [^{18}F]GSK1482160 SUVR was greater in the cortex and basal forebrain system of 7-month-old rTg4510 mice than in age-matched wild-type mice (Figure 1b,f,g) and was greater in the cortex, basal forebrain system, striatum and amygdala of 7-month-old rTg4510 mice than in 3-month-old rTg4510 mice (Figure 1e−g).

To understand the link between tau accumulation and P2X7R alterations in the brain, we performed correlation analysis between [^{18}F]GSK1482160 and the tau tracer [^{18}F]APN-1607 in 11 rTg4510 mice (including five 3 months of age and six 7 months of age). The description for radiosynthesis and the mciroPET method for [^{18}F]APN-1607 imaging in rTg4510 mice and wild-type mice can be found in.[35] The data for [^{18}F]APN-1607 SUVR (with Cb as the reference region) in the same rTg4510 mice were obtained from our recent study.[35] Nonparametric Spearman's rank analysis revealed a positive correlation between tau [^{18}F]APN-1607 uptake and [^{18}F]GSK1482160 uptake in the hippocampus of rTg4510 mice (r = 0.6909, p = 0.0226, n = 11, Figure 1i)

The Uptake of [^{18}F]GSK1482160 Did Not Differ between APP/PS1, 5×FAD, and 3×Tg Mice and Age-Matched Wild-Type Mice. Next, we assessed the changes in the level of P2X7R in the brains of mouse models of AD amyloidosis. 5×FAD mice develop Aβ plaques at approximately 5 months of age. Here, we chose 3 months and 7 months as the pre- and postpathological time points, respectively. Here, we found that there was no difference in the [^{18}F]GSK1482160 SUVR in the brains of 5×FAD mice (3 and 7 months) compared to age-matched wild-type mice (Figure 1a−d,g). APP/PS1 mice develop Aβ plaques at approximately 6 months of age. 3×Tg mice are models of both cerebral Aβ plaques and tau pathology; however, due to genetic drift, recent studies from our group and other groups have shown limited pathology at the age of 10 months.[31] Here, we chose APP/PS1 mice at 5 and 10 months of age and 3×Tg mice at 10 months of age for [^{18}F]GSK1482160 imaging. We observed no difference in [^{18}F]GSK1482160 SUVR in other mouse models of APP/PS1 (5 and 10 months) (Figure 2) or in 3×Tg mice (10 months) (Figure 2). There was overall increase in regional [^{18}F]GSK1482160 SUV in the brain from 5 month old APP/PS1 mice compared to age-matched wild-type mice, however the regional [^{18}F]GSK1482160 SUVR

https://doi.org/10.1021/acschemneuro.4c00067
ACS Chem. Neurosci. 2024, 15, 2112−2120

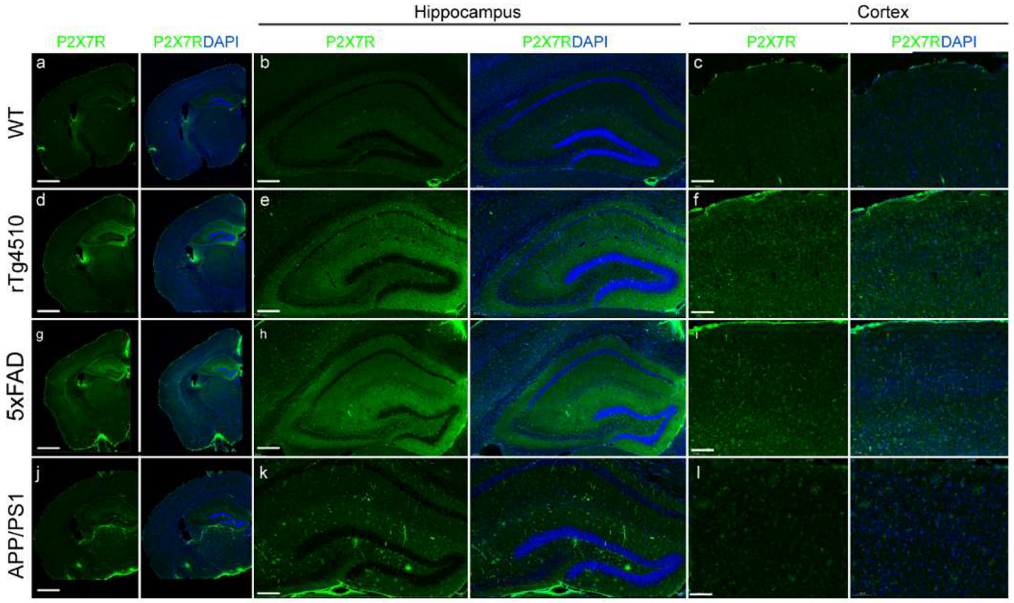

Figure 4. Representative P2X7R staining of coronal brain slices from WT, rTg4510, 5×FAD, and APP/PS1 mice. (a, d, g, j) Overview and (b, c, e, f, h, i, k, l) zoomed-in view revealing the distribution of P2X7Rs (green) in the hippocampus (Hip) and cortex (Ctx) of 7-month-old WT (a−c), 7-month-old rTg4510 (d−f), 7-month-old 5×FAD (g−i), and 10-month-old APP/PS1 mice. Nuclei were counterstained with DAPI (blue). Scale bar = 1 mm (a, d, g, j), 200 μm (c, f, i, l), 100 μm (b, e, h, k).

(cerebellum as reference region) was comparable between two groups (Figure S3).

P2X7R Distribution in the Mouse Brain. Ex vivo immunofluorescence staining was performed on mouse brain tissue slices after in vivo imaging. The P2X7R signals in the brains of APP/PS1 mice and WT mice appeared comparable. The accumulation of tau inclusion was validated by using phospho-Tau staining of brain tissue slices from 7-month-old rTg4510 mice and WT mice (Figure 3a−c). Tau tangles and were detected in the cortex and hippocampus of 7-month-old rTg4510 mice. Amyloid-beta deposits were detected in the cortex, hippocampus and thalamus of both 5×FAD mice at 7 months of age (Figure 3d−f) and 10-month-old APP/PS1 mice at 10 months of age (Figure 3g−i). The P2X7R signal in the brains of the rTg4510 mice was higher in the hippocampus than in the cortex based on the ex vivo staining, which was slightly different from the in vivo pattern (Figure 4a−l).

Here, we found increased regional [^{18}F]GSK1482160 uptake in the cortical and subcortical regions of P2X7Rs in 7-month-old rTg4510 mice compared to age-matched controls and 3-month-old rTg4510 mice. No difference in the regional [^{18}F]GSK1482160 SUVR was observed in the brains of APP/PS1 mice (5 and 10 months), 5×FAD mice (3 and 7 months), or 3×Tg mice (10 months) compared to age-matched wild-type mice. The pharmacokinetics of [^{18}F]-GSK1482160 in rodents as well as test-retest of the tracer has been reported in our studies.[25,36]

rTg4510 mice develop tau deposits at 4−5 months of age, which can be detected by PET using [^{11}C]PBB3 and [^{18}F]PM-PBB3 ([^{18}F]APN-1607).[33] In vivo imaging using [^{18}F]DPA-714 and [^{11}C]AC-5216 has shown increases in TSPO (representing microgliosis) along with tau accumulation.[33,34] In addition, genome-wide RNaseq studies and ex vivo staining have demonstrated increased immunoreactivity for the astrocyte and the microglial marker in the brains of rTg4510 mice.[37] Tau pathology has been shown to epigenetically remodel neuron-glial cross-talk in AD A recent study showed that the RNA level was increased in the brain of rTg4510 mice at 6 months and that P2X7R influences the tau aggregate burden in human tauopathies and induces distinct signaling in microglia and astrocytes.[7] Our observation of an increase in P2X7R by PET using [^{18}F]GSK1482160 in tauopathy mouse brain is in line with the existing autoradiographic study using [^{123}I]TZ6019 in the brain tissue from 9-month-old PS19 (P301S tau) mice, with an approximately 35% increase compared to age-matched wild-type mice.[18]

In contrast to the increase observed in tau rTg4510 mice, we found no clear difference in [^{18}F]GSK1482160 uptake in the brains of 3- or 7-month-old 5×FAD mice. Similar observation was reported in an earlier immunostaining study showing the opposite pattern in P2X7R signaling, with an increase in the brains of tauopathy P301S mice and a reduction in the brains of 5×FAD mice in the same study.[38] Another study revealed that P2X7R protein expression in the frontal cortex was approximately 150% greater in 9-month-old 5×FAD mice than in 3-month-old 5×FAD mice and was greater than in wild-type mice.[39]

For APP/PS1 mice, regional P2X7Rs in the brains of 5-month-old and 10-month-old APP/PS1 mice were comparable to those in age-matched wild-type mice by using [^{18}F]-GSK1482160. To date, only one in vivo study of [^{18}F]4A PET has been performed in a 12- to 13-month-old APP/PS1 mouse model,[26] with the highest binding observed in the anterior commissure, putamen, neocortex and medulla, followed by the cerebellum. Despite the increased area under the curve, the SUVRs (relative to the cerebellum) were comparable between 12- to 13-month-old APP/PS1 and wild-type mice.[26] An earlier study showed that immunofluorescence staining of P2X7Rs increased by 20% in the cortex and 30% in the hippocampus of 10-month-old APP/PS1 mice compared to wild-type mice,[4] while another Western blot analysis showed that P2X7Rs were more abundant in the cortex of 6-month-old and 12-month-old APP/PS1 mice compared to nontransgenic littermates.[40] Transcriptomic analysis of the levels of *p2rx7* in 2-, 10- and

https://doi.org/10.1021/acschemneuro.4c00067
ACS Chem. Neurosci. 2024, 15, 2112−2120

20-month-old 3×Tg mice did not reveal a significant difference.[41]

There are several limitations in the current study. First, sex differences in the expression of P2X7Rs in mouse brains have not been studied. Second, this study was cross-sectional rather than longitudinal. Further longitudinal assessments in the same set of animal models will be informative. Third, the PET scans are not dynamic; therefore, BPnd readouts were not available. Moreover, P2X7R expression is highly dependent on the activation state of microglia, and further detailed profiling of microglia in relation to in vivo P2X7R tracer uptake is needed. We used PMOD small animal brain atlas based analysis for quantification. This approach is widely used in small animal PET data analysis. SPM based analysis provides insightful voxel-based analysis. Based on earlier publications, the quantification using SPM and PMOD are comparable. Both methods have shown effectiveness in analyzing animal PET imaging data.

In conclusion, these findings provide in vivo imaging evidence for diverse patterns of P2X7R, with increased P2X7R in the widely used rTg4510 model of 4-repeat tauopathy but not in the amyloidosis models 5×FAD, APP/PS1 or 3×Tg mice. [^{18}F]GSK1482160 imaging might be useful for in vivo evaluation of neuroinflammation in neurodegenerative diseases.

METHODS

Animal Models. The animal models used in this study are summarized in Table 1. Sixty mice were included in total, including rTg4510 mice [STOCK Tg(Camk2a-tTA)1Mmay Fgf14Tg(tetO-MAPT*P301L)4510Kha/J] (Jax Laboratory),[32] APP/PS1 mice [B6.Cg-Tg(APPswe,PSEN 1dE9)85Dbo/Mmjax],[27] 3×Tg mice [B6;129-Psen1tm1MpmTg(APPSwe, tauP301L)1Lfa/Mmjax] (Jax Laboratory),[30] and 5×FAD mice [B6. Cg-Tg(APPSwFlLon,-PSEN1*M146L*L286V)6799Vas/Mmjax] (Jax Laboratory).[42] Wild-type C57BL6 mice were obtained from Charles River, Germany, and Cavins Laboratory Animal Co., Ltd., of Changzhou. Mice were housed in ventilated cages inside a temperature-controlled room under a 12 h dark/light cycle. Pelleted food and water were provided ad libitum. Paper tissue and red mouse house shelters were placed in cages for environmental enrichment. The in vivo PET imaging and experimental protocol were approved by the Institutional Animal Care and Ethics Committee of Huashan Hospital of Fudan University and Sun Yat-sen University and performed in accordance with the National Research Council's Guide for the Care and Use of Laboratory Animals. All experiments were carried out in compliance with national laws for animal experimentation and were approved by the Animal Ethics Committee of Fudan University and Sun Yat-Sen University. All of the experiments were carried out in compliance with ARRIVE guidelines 2.0, the national laws for animal experimentation.

Table 1. Information on the Animal Models Used in the Study[a]

animal model	age (month)	[^{18}F]GSK1482160 PET	[^{18}F]APN-1607 PET
WT	3	4 M	
	5	5 M	
	7	5 M	
	10	5 M	
rTg4510	3	6 M	5 M
	7	8 M	6 M
APP/PS1	5	6 M	
	10	10 M	
3×Tg	10	3 M	
5×FAD	3	3 M/3 F	
	7	3 M/3 F	

[a]M: male. F: female. Sixty mice were included. Detailed [^{18}F]APN-1607 PET method and data can be found in ref 35.

Radiosynthesis. [^{18}F]GSK1482160 was synthesized and radiolabeled based on nucleophilic aliphatic substitution according to protocols described previously. The identities of the final products were confirmed by comparison with the HPLC retention times of the nonradioactive reference compounds obtained by coinjection using a Luna 5 μm C18(2) 100 Å (250 mm × 4.6 mm) column (Phenomenex) with acetonitrile and water (60:40) as the solvent and a 1.0 mL/min flow rate. A radiochemical purity >95% was achieved for [^{18}F]GSK1482160 (molar activity, 1.48 GBq/mL)[26] (the HPLC results are shown in Figure S1).

Small Animal PET. PET experiments were performed using a Siemens Inveon PET/computed tomography (CT) system (Siemens Medical Solutions, Knoxville, TN, United States). Prior to the scans, the mice were anesthetized using isoflurane (2.0−3.0%) in medical oxygen (1 L/min) at room temperature with an isoflurane vaporizer (Molecular Imaging Products Company, United States). The mice were positioned in a spread-up position on the imaging bed and subjected to inhalation of the anesthetic (1.5−2.5% isoflurane) during the PET/CT procedure.[43] A single dose of [^{18}F]GSK1482160 (~0.37 MBq/g body weight, 0.1−0.2 mL) was injected into the animals through the tail vein under isoflurane anesthesia. Static PET/CT images were obtained 10 min after intravenous administration of [^{18}F]GSK1482160 for 50−60 min. PET/CT images were reconstructed using the ordered subset expectation maximization 3D algorithm (OSEM3D), with a matrix size of 128 × 128 × 159 and a voxel size of 0.815 mm × 0.815 mm × 0.796 mm. The data were reviewed using Inveon Research Workplace (IRW) software (Siemens, United States). Attenuation corrections derived from hybrid CT data were applied.

Imaging Data Analysis. The images were processed and analyzed using PMOD 4.4 software (PMOD Technologies Ltd., Zurich, Switzerland). The time−activity curves were deduced from specific volumes of interest that were defined based on mouse magnetic resonance imaging T_2-weighted images and the Ma-Benveniste-Mirrione atlas (in PMOD). Radioactivity is presented as the standardized uptake value (SUV) (decay-corrected radioactivity per cm^3 divided by the injected dose per gram of body weight). The brain regional SUVRs were calculated using the cerebellum (Cb) as the reference region as described in an earlier PET study using [^{18}F]JNJ-64413739 in rodents.[23] A mask was applied for signals outside the brain volumes of interest for illustration. To understand the link between tau deposits and P2X7R alterations in the brain, we performed nonparametric Spearman's correlation analysis between the uptake of [^{18}F]GSK1482160 and the tau tracer [^{18}F]APN-1607 in the brain of rTg4510 mice. Data for [^{18}F]APN-1607 SUVR (with Cb as the reference region) in the same rTg4510 mice (3 and 7 months of age) that underwent [^{18}F]GSK1482160 imaging were obtained from an earlier study (detailed information in Table 1).[35]

Immunofluorescence Staining. After in vivo imaging, the mice were anesthetized with tribromoethanol, perfused with ice-cold 0.1 M phosphate buffered saline (PBS, pH 7.4) and 4% paraformaldehyde in 0.1 M PBS (pH 7.4), fixed for 36 h in 4% paraformaldehyde (pH 7.4), and subsequently stored in 0.1 M PBS (pH 7.4) at 4 °C. The brain was placed in 30% sucrose in PBS until it sank. The brain was embedded in OCT gel (Tissue-Tek O.C.T., Sakura, USA). Coronal brain sections (20 μm) were cut around the bregma 0 to −2 mm using a Leica CM1950 cryostat (Leica Biosystems, Germany). For P2X7R immunofluorescence labeling, sections were blocked in blocking buffer containing 3% bovine serum albumin (BSA), 0.4% Triton X-100, and 5% normal goat serum (NGS) in PBS for 2 h at room temperature. After washing with PBS for 3 × 10 min, the sections were incubated with primary antibodies in blocking buffer overnight at 4 °C, incubated with donkey anti-rat IgG H&L (Alexa Fluor 647) (1:500, ab150155, Abcam) in blocking buffer for 2 h at room temperature and subsequently washed with PBS for 3 × 10 min.

https://doi.org/10.1021/acschemneuro.4c00067
ACS Chem. Neurosci. 2024, 15, 2112−2120

For Aβ and tau staining, coronal brain sections (3 μm) were cut using a Leica RM2016 microtome (Leica, Germany). The sections were first washed in PBS 3 × 10 min, followed by antigen retrieval for 20 min in citrate buffer (pH 6.0) at room temperature. After antigen retrieval in citrate buffer at room temperature, the sections were permeabilized and blocked in 3% bovine serum albumin for 30 min at room temperature with mild shaking. Paraffine-embedded sections were incubated overnight at 4 °C with primary antibodies against Aβ and phospho-Tau (Ser202, Thr205). The next day, the slices were washed with PBS 3 × 5 min, incubated with secondary antibody for 2 h at room temperature, and washed 3 × 5 min with PBS. The sections were incubated for 10 min in 4′,6-diamidino-2-phenylindole (DAPI) at room temperature and mounted with antifade mounting media. The brain sections were imaged at ×20 magnification using a Pannoramic MIDI slide scanner (3DHISTECH) with the same acquisition settings for all brain slices. The images were analyzed by using ImageJ (NIH, U.S.A.). Antibodies used in the immunofluorescence staining were listed in Table S1.

Statistics. Two-way ANOVA with Sidak's post hoc analysis was used for comparisons between groups (GraphPad Prism 9.0, CA, USA). Nonparametric Spearman's rank correlation analysis was used to analyze the associations between the regional SUVRs of [^{18}F]GSK1482160 and [^{18}F]APN-1607. A p value less than 0.05 was considered to indicate statistical significance. The data are shown as the mean ± standard deviation.

■ ASSOCIATED CONTENT

Supporting Information

The Supporting Information is available free of charge at https://pubs.acs.org/doi/10.1021/acschemneuro.4c00067.

HPLC chromatogram of synthesized [^{18}F]GSK1482160 and the standard; unmasked [^{18}F]GSK1482160 PET images overlaid on MRI template of a wild-type mouse showing lower brain tracer uptake than outside the brain; quantification of [^{18}F]GSK1482160 SUV in the brain of WT, rTg4510, 5×FAD, APP/PS1, and 3×Tg mice; details on the antibodies and reagents used for immunofluorescence staining (PDF)

■ AUTHOR INFORMATION

Corresponding Authors

Hongjun Jin − *Guangdong Provincial Engineering Research Center of Molecular Imaging, The Fifth Affiliated Hospital, Sun Yat-Sen University, Zhuhai, Guangdong 519000, China*; orcid.org/0000-0002-1522-1098; Email: jinhj3@mail.sysu.edu.cn

Ruiqing Ni − *Institute for Regenerative Medicine, University of Zurich, Zurich 8952, Switzerland; Department of Nuclear Medicine, University Hospital, Inselspital Bern, Bern 3010, Switzerland; Institute for Biomedical Engineering, University of Zurich & ETH Zurich, Zurich 8093, Switzerland*; orcid.org/0000-0002-0793-2113; Email: ni@biomed.ee.ethz.ch

Authors

Yanyan Kong − *PET Center, Huashan Hospital, Fudan University, Shanghai 200235, China*

Lei Cao − *PET Center, Huashan Hospital, Fudan University, Shanghai 200235, China; Institute for Regenerative Medicine, University of Zurich, Zurich 8952, Switzerland*

Jiao Wang − *Lab of Molecular Neural Biology, School of Life Sciences, Shanghai University, Shanghai 200444, China*

Junyi Zhuang − *Lab of Molecular Neural Biology, School of Life Sciences, Shanghai University, Shanghai 200444, China*

Yongshan Liu − *Guangdong Provincial Engineering Research Center of Molecular Imaging, The Fifth Affiliated Hospital, Sun Yat-Sen University, Zhuhai, Guangdong 519000, China*

Lei Bi − *Guangdong Provincial Engineering Research Center of Molecular Imaging, The Fifth Affiliated Hospital, Sun Yat-Sen University, Zhuhai, Guangdong 519000, China*

Yifan Qiu − *Guangdong Provincial Engineering Research Center of Molecular Imaging, The Fifth Affiliated Hospital, Sun Yat-Sen University, Zhuhai, Guangdong 519000, China*

Yuyi Hou − *Guangdong Provincial Engineering Research Center of Molecular Imaging, The Fifth Affiliated Hospital, Sun Yat-Sen University, Zhuhai, Guangdong 519000, China*

Qi Huang − *PET Center, Huashan Hospital, Fudan University, Shanghai 200235, China*

Fang Xie − *PET Center, Huashan Hospital, Fudan University, Shanghai 200235, China*

Yunhao Yang − *PET Center, Huashan Hospital, Fudan University, Shanghai 200235, China*

Kuangyu Shi − *Department of Nuclear Medicine, University Hospital, Inselspital Bern, Bern 3010, Switzerland*

Axel Rominger − *Department of Nuclear Medicine, University Hospital, Inselspital Bern, Bern 3010, Switzerland*

Yihui Guan − *PET Center, Huashan Hospital, Fudan University, Shanghai 200235, China*

Complete contact information is available at: https://pubs.acs.org/10.1021/acschemneuro.4c00067

Author Contributions

The study was designed by Y.K. and R.N. Y.K. performed the radiolabeling, HPLC, and small animal PET. L.C. and R.N. performed the small animal PET analysis. Y.L., Y.H., Y.Q., and L.B. provided support for the PET data analysis. Y.K. and R.N. wrote the first draft. H.J. provided GSK1482160 precursor and methodology for radiolabeling. All the authors contributed to the revision of the manuscript. All the authors have read and approved the final manuscript.

Funding

Y.K. received funding from the National Natural Science Foundation of China (Grants 82272108 and 81701732), the Natural Science Foundation of Shanghai (Grant 22ZR1409200), and the Shanghai Science and Technology Innovation Action Plan Medical Innovation Research Project (Grant 23Y11903200). Y.G. received funding from the NSFC (Grant 82071962). H.J. received funding from the National Natural Science Foundation of China (Grants 82150610508, 82372004, and 81871382), the Key Realm R&D Program of Guangdong Province (Grant 2018B030337001), the Guangdong Provincial Basic and Applied Basic Research Fund Provincial Enterprise Joint Fund (Grant 2021A1515220004), and the Guangdong-Hong Kong Macao University Joint Laboratory of Interventional Medicine Foundation of Guangdong Province (Grant 2023LSYS001). R.N. received funding from the Swiss Center for Applied Human Toxicology (Grant AP22_02) and Helmut Horten Stiftung.

Notes

The authors declare no competing financial interest.

■ ACKNOWLEDGMENTS

The authors thank Dr. Jianfei Xiao, PET Center, Huashan Hospital, Fudan University, for assisting with the radiolabeling and HPLC.

ABBREVIATIONS

AD, Alzheimer's disease
FTLD, frontotemporal lobar degeneration
CBD, corticobasal degeneration
PSP, progressive supranuclear palsy
P2X7R, purinergic receptor P2X7
PET, positron emission tomography
TSPO, translocator protein
HPLC, high-performance liquid chromatography

REFERENCES

(1) Di Virgilio, F.; Dal Ben, D.; Sarti, A. C.; Giuliani, A. L.; Falzoni, S. The P2X7 Receptor in Infection and Inflammation. *Immunity* **2017**, *47* (1), 15−31. From NLM.

(2) Beltran-Lobo, P.; Reid, M. J.; Jimenez-Sanchez, M.; Verkhratsky, A.; Perez-Nievas, B. G.; Noble, W. Astrocyte adaptation in Alzheimer's disease: a focus on astrocytic P2X7R. *Essays Biochem* **2023**, *67* (1), 119−130. From NLM.

(3) Carvalho, K.; Martin, E.; Ces, A.; Sarrazin, N.; Lagouge-Roussey, P.; Nous, C.; Boucherit, L.; Youssef, I.; Prigent, A.; Faivre, E.; et al. P2X7-deficiency improves plasticity and cognitive abilities in a mouse model of Tauopathy. *Prog. Neurobiol* **2021**, *206*, No. 102139. From NLM.

(4) Martin, E.; Amar, M.; Dalle, C.; Youssef, I.; Boucher, C.; Le Duigou, C.; Brückner, M.; Prigent, A.; Sazdovitch, V.; Halle, A.; et al. New role of P2X7 receptor in an Alzheimer's disease mouse model. *Mol. Psychiatry* **2019**, *24* (1), 108−125. From NLM.

(5) Miras-Portugal, M. T.; Diaz-Hernandez, J. I.; Gomez-Villafuertes, R.; Diaz-Hernandez, M.; Artalejo, A. R.; Gualix, J. Role of P2X7 and P2Y2 receptors on α-secretase-dependent APP processing: Control of amyloid plaques formation "in vivo" by P2X7 receptor. *Comput. Struct Biotechnol J.* **2015**, *13*, 176−181. From NLM.

(6) Diaz-Hernandez, J. I.; Gomez-Villafuertes, R.; León-Otegui, M.; Hontecillas-Prieto, L.; Del Puerto, A.; Trejo, J. L.; Lucas, J. J.; Garrido, J. J.; Gualix, J.; Miras-Portugal, M. T.; et al. In vivo P2X7 inhibition reduces amyloid plaques in Alzheimer's disease through GSK3β and secretases. *Neurobiol Aging* **2012**, *33* (8), 1816−1828. From NLM.

(7) Beltran-Lobo, P.; Hughes, M. M.; Troakes, C.; Croft, C. L.; Rupawala, H.; Jutzi, D.; Ruepp, M. D.; Jimenez-Sanchez, M.; Perkinton, M. S.; Kassiou, M.; et al. P2X(7)R influences tau aggregate burden in human tauopathies and shows distinct signalling in microglia and astrocytes. *Brain Behav Immun* **2023**, *114*, 414−429. From NLM.

(8) McLarnon, J. G.; Ryu, J. K.; Walker, D. G.; Choi, H. B. Upregulated expression of purinergic P2X(7) receptor in Alzheimer disease and amyloid-beta peptide-treated microglia and in peptide-injected rat hippocampus. *J. Neuropathol Exp Neurol* **2006**, *65* (11), 1090−1097. From NLM.

(9) Martínez-Frailes, C.; Di Lauro, C.; Bianchi, C.; de Diego-García, L.; Sebastián-Serrano, Á.; Boscá, L.; Díaz-Hernández, M. Amyloid Peptide Induced Neuroinflammation Increases the P2X7 Receptor Expression in Microglial Cells, Impacting on Its Functionality. *Front Cell Neurosci* **2019**, *13*, 143. From NLM.

(10) Ruan, Z.; Delpech, J. C.; Venkatesan Kalavai, S.; Van Enoo, A. A.; Hu, J.; Ikezu, S.; Ikezu, T. P2RX7 inhibitor suppresses exosome secretion and disease phenotype in P301S tau transgenic mice. *Mol. Neurodegener* **2020**, *15* (1), 47. From NLM.

(11) Bianchi, C.; Alvarez-Castelao, B.; Sebastián-Serrano, Á.; Di Lauro, C.; Soria-Tobar, L.; Nicke, A.; Engel, T.; Díaz-Hernández, M. P2X7 receptor inhibition ameliorates ubiquitin-proteasome system dysfunction associated with Alzheimer's disease. *Alzheimers Res. Ther* **2023**, *15* (1), 105. From NLM.

(12) Schmidt, S.; Isaak, A.; Junker, A. Spotlight on P2X7 Receptor PET Imaging: A Bright Target or a Failing Star? *Int. J. Mol. Sci.* **2023**, *24* (2), 1374. From NLM.

(13) Crabbé, M.; Van der Perren, A.; Bollaerts, I.; Kounelis, S.; Baekelandt, V.; Bormans, G.; Casteels, C.; Moons, L.; Van Laere, K. Increased P2X7 Receptor Binding Is Associated With Neuroinflammation in Acute but Not Chronic Rodent Models for Parkinson's Disease. *Frontiers in Neuroscience* **2019**, *13*, 799.

(14) Huang, G.; Lu, X.; Qiu, Y.; Bi, L.; Ye, P.; Yang, M.; Shen, Y.; Jin, H.; Han, J. Hetero-aryl bromide precursor fluorine-18 radiosynthesis and preclinical evaluation of a novel positron emission tomography (PET) tracer [(18)F]GSK1482160. *Bioorg. Med. Chem.* **2022**, *73*, No. 116996. From NLM.

(15) Janssen, B.; Vugts, D. J.; Wilkinson, S. M.; Ory, D.; Chalon, S.; Hoozemans, J. J. M.; Schuit, R. C.; Beaino, W.; Kooijman, E. J. M.; van den Hoek, J.; et al. Identification of the allosteric P2X7 receptor antagonist [11C]SMW139 as a PET tracer of microglial activation. *Sci. Rep.* **2018**, *8* (1), 6580.

(16) Gao, M.; Wang, M.; Glick-Wilson, B. E.; Meyer, J. A.; Peters, J. S.; Territo, P. R.; Green, M. A.; Hutchins, G. D.; Zarrinmayeh, H.; Zheng, Q. H. Synthesis and preliminary biological evaluation of a novel P2X7R radioligand [(18)F]IUR-1601. *Bioorg. Med. Chem. Lett.* **2018**, *28* (9), 1603−1609. From NLM.

(17) Janssen, B.; Vugts, D. J.; Funke, U.; Spaans, A.; Schuit, R. C.; Kooijman, E.; Rongen, M.; Perk, L. R.; Lammertsma, A. A.; Windhorst, A. D. Synthesis and initial preclinical evaluation of the P2X7 receptor antagonist [^{11}C]A-740003 as a novel tracer of neuroinflammation. *J. Labelled Comp Radiopharm* **2014**, *57* (8), 509−516. From NLM.

(18) Jin, H.; Han, J.; Resing, D.; Liu, H.; Yue, X.; Miller, R. L.; Schoch, K. M.; Miller, T. M.; Perlmutter, J. S.; Egan, T. M.; et al. Synthesis and in vitro characterization of a P2X7 radioligand [(123)I]TZ6019 and its response to neuroinflammation in a mouse model of Alzheimer disease. *Eur. J. Pharmacol.* **2018**, *820*, 8−17. From NLM.

(19) Fu, Z.; Lin, Q.; Hu, B.; Zhang, Y.; Chen, W.; Zhu, J.; Zhao, Y.; Choi, H. S.; Shi, H.; Cheng, D. P2X7 PET Radioligand (18)F-PTTP for Differentiation of Lung Tumor from Inflammation. *J. Nucl. Med.* **2019**, *60* (7), 930−936. From NLM.

(20) Fu, Z.; Lin, Q.; Xu, Z.; Fu, W.; Shi, D.; Cheng, Y.; Yang, T.; Liu, G.; Shi, H.; Cheng, D. Longitudinal Positron Emission Tomography Imaging with P2X7 Receptor-Specific Radioligand (18)F-FTTM in a Kainic Acid Rat Model of Temporal Lobe Epilepsy. *ACS Chem. Neurosci.* **2022**, *13* (23), 3512−3522. From NLM.

(21) Alzghool, O. M.; Aarnio, R.; Helin, J. S.; Wahlroos, S.; Keller, T.; Matilainen, M.; Solis, J.; Danon, J. J.; Kassiou, M.; Snellman, A.; et al. Glial reactivity in a mouse model of beta-amyloid deposition assessed by PET imaging of P2X7 receptor and TSPO using [(11)C]SMW139 and [(18)F]F-DPA. *EJNMMI Res.* **2024**, *14* (1), 25. From NLM.

(22) Morgan, J.; Moreno, O.; Alves, M.; Baz, Z.; Menéndez Méndez, A.; Leister, H.; Melia, C.; Smith, J.; Visekruna, A.; Nicke, A.; et al. Increased uptake of the P2X7 receptor radiotracer (18) F-JNJ-64413739 in the brain and peripheral organs according to the severity of status epilepticus in male mice. *Epilepsia* **2023**, *64* (2), 511−523. From NLM.

(23) Berdyyeva, T.; Xia, C.; Taylor, N.; He, Y.; Chen, G.; Huang, C.; Zhang, W.; Kolb, H.; Letavic, M.; Bhattacharya, A.; et al. PET Imaging of the P2X7 Ion Channel with a Novel Tracer [(18)F]JNJ-64413739 in a Rat Model of Neuroinflammation. *Mol. Imaging Biol.* **2019**, *21* (5), 871−878. From NLM.

(24) Territo, P. R.; Meyer, J. A.; Peters, J. S.; Riley, A. A.; McCarthy, B. P.; Gao, M.; Wang, M.; Green, M. A.; Zheng, Q. H.; Hutchins, G. D. Characterization of (11)C-GSK1482160 for Targeting the P2X7 Receptor as a Biomarker for Neuroinflammation. *J. Nucl. Med.* **2017**, *58* (3), 458−465. From NLM.

(25) Zhang, S.; Qiu, Y.; Huang, L.; Bi, L.; Guo, Y.; You, K.; Huang, G.; Wang, Y.; Lu, H.; Jin, H.; et al. Ankylosing spondylitis PET imaging and quantifications via P2X7 receptor-targeting radioligand [(18)F]GSK1482160. *Eur. J. Nucl. Med. Mol. Imaging* **2023**, *50*, 3589. From NLM.

https://doi.org/10.1021/acschemneuro.4c00067
ACS Chem. Neurosci. 2024, 15, 2112−2120

(26) Huang, G.; Qiu, Y.; Bi, L.; Wei, H.; Li, G.; Li, Z.; Ye, P.; Yang, M.; Shen, Y.; Liu, H.; et al. PET Imaging of P2X7 Receptor (P2X7R) for Neuroinflammation with Improved Radiosynthesis of Tracer [(18)F]4A in Mice and Non-human Primates. *ACS Chem. Neurosci.* **2022**, *13* (23), 3464−3476. From NLM.
(27) Jankowsky, J. L.; Fadale, D. J.; Anderson, J.; Xu, G. M.; Gonzales, V.; Jenkins, N. A.; Copeland, N. G.; Lee, M. K.; Younkin, L. H.; Wagner, S. L.; et al. Mutant presenilins specifically elevate the levels of the 42 residue beta-amyloid peptide in vivo: evidence for augmentation of a 42-specific gamma secretase. *Hum. Mol. Genet.* **2004**, *13* (2), 159−170. From NLM.
(28) Jawhar, S.; Trawicka, A.; Jenneckens, C.; Bayer, T. A.; Wirths, O. Motor deficits, neuron loss, and reduced anxiety coinciding with axonal degeneration and intraneuronal Aβ aggregation in the 5XFAD mouse model of Alzheimer's disease. *Neurobiol. Aging* **2012**, *33* (1), 196.e29. From NLM.
(29) Forner, S.; Kawauchi, S.; Balderrama-Gutierrez, G.; Kramár, E. A.; Matheos, D. P.; Phan, J.; Javonillo, D. I.; Tran, K. M.; Hingco, E.; da Cunha, C.; et al. Systematic phenotyping and characterization of the 5xFAD mouse model of Alzheimer's disease. *Sci. Data* **2021**, *8* (1), 270. From NLM.
(30) Oddo, S.; Caccamo, A.; Shepherd, J. D.; Murphy, M. P.; Golde, T. E.; Kayed, R.; Metherate, R.; Mattson, M. P.; Akbari, Y.; LaFerla, F. M. Triple-transgenic model of Alzheimer's disease with plaques and tangles: intracellular Abeta and synaptic dysfunction. *Neuron* **2003**, *39* (3), 409−421. From NLM.
(31) Javonillo, D. I.; Tran, K. M.; Phan, J.; Hingco, E.; Kramár, E. A.; da Cunha, C.; Forner, S.; Kawauchi, S.; Milinkeviciute, G.; Gomez-Arboledas, A.; et al. Systematic Phenotyping and Characterization of the 3xTg-AD Mouse Model of Alzheimer's Disease. *Front Neurosci* **2022**, *15*, No. 785276. From NLM.
(32) Santacruz, K.; Lewis, J.; Spires, T.; Paulson, J.; Kotilinek, L.; Ingelsson, M.; Guimaraes, A.; DeTure, M.; Ramsden, M.; McGowan, E.; et al. Tau suppression in a neurodegenerative mouse model improves memory function. *Science* **2005**, *309* (5733), 476−481. From NLM.
(33) Ishikawa, A.; Tokunaga, M.; Maeda, J.; Minamihisamatsu, T.; Shimojo, M.; Takuwa, H.; Ono, M.; Ni, R.; Hirano, S.; Kuwabara, S.; et al. In Vivo Visualization of Tau Accumulation, Microglial Activation, and Brain Atrophy in a Mouse Model of Tauopathy rTg4510. *J. Alzheimers Dis* **2018**, *61* (3), 1037−1052. From NLM.
(34) Endepols, H.; Anglada-Huguet, M.; Mandelkow, E.; Schmidt, Y.; Krapf, P.; Zlatopolskiy, B. D.; Neumaier, B.; Mandelkow, E.-M.; Drzezga, A. Assessment of the In Vivo Relationship Between Cerebral Hypometabolism, Tau Deposition, TSPO Expression, and Synaptic Density in a Tauopathy Mouse Model: a Multi-tracer PET Study. *Molecular Neurobiology* **2022**, *59* (6), 3402−3413.
(35) Kong, Y.; Xie, F.; Wang, X.; Zuo, C.; Huang, Q.; Shi, K.; Rominger, A.; Xiao, J.; Li, M.; Wu, P.; et al. In vivo reactive astrocyte imaging using [18F]SMBT-1 in tauopathy and familial Alzheimer's disease mouse models - a multitracer study. *Res. Square* **2023**, DOI: 10.21203/rs.3.rs-3415769/v1.
(36) Zhou, R.; Ji, B.; Kong, Y.; Qin, L.; Ren, W.; Guan, Y.; Ni, R. PET Imaging of Neuroinflammation in Alzheimer's Disease. *Frontiers in Immunology* **2021**, *12*, 3750.
(37) Wang, H.; Li, Y.; Ryder, J. W.; Hole, J. T.; Ebert, P. J.; Airey, D. C.; Qian, H. R.; Logsdon, B.; Fisher, A.; Ahmed, Z.; et al. Genome-wide RNAseq study of the molecular mechanisms underlying microglia activation in response to pathological tau perturbation in the rTg4510 tau transgenic animal model. *Mol. Neurodegener* **2018**, *13* (1), 65. From NLM.
(38) Gomez-Gutierrez, R.; Fujita, M.; Jankowsky, J. L. TSPO and P2X7 discriminate between amyloid- and tau-induced glial responses. *Alzheimer's Dementia* **2021**, *17* (S5), No. e058697. Accessed Oct 8, 2023.
(39) Islam, J.; Cho, J. A.; Kim, J. Y.; Park, K. S.; Koh, Y. J.; Chung, C. Y.; Lee, E. J.; Nam, S. J.; Lee, K.; Kim, S. H.; et al. GPCR19 Regulates P2X7R-Mediated NLRP3 Inflammasomal Activation of Microglia by Amyloid β in a Mouse Model of Alzheimer's Disease. *Front Immunol* **2022**, *13*, No. 766919. From NLM.
(40) Lee, H. G.; Won, S. M.; Gwag, B. J.; Lee, Y. B. Microglial $P2X_7$ receptor expression is accompanied by neuronal damage in the cerebral cortex of the APPswe/PS1dE9 mouse model of Alzheimer's disease. *Exp Mol. Med.* **2011**, *43* (1), 7−14. From NLM.
(41) Lambracht-Washington, D.; Fu, M.; Manouchehri, N.; Hynan, L. S.; Stuve, O.; Rosenberg, R. N. Glial cell transcriptome analyses in 3xTg-AD mice: Effects of aging, disease progression, and anti-Aβ immunotherapy. *Aging Brain* **2023**, *3*, No. 100066. From NLM.
(42) Oakley, H.; Cole, S. L.; Logan, S.; Maus, E.; Shao, P.; Craft, J.; Guillozet-Bongaarts, A.; Ohno, M.; Disterhoft, J.; Van Eldik, L.; et al. Intraneuronal beta-amyloid aggregates, neurodegeneration, and neuron loss in transgenic mice with five familial Alzheimer's disease mutations: potential factors in amyloid plaque formation. *J. Neurosci.* **2006**, *26* (40), 10129−10140. From NLM.
(43) Kong, Y.; Maschio, C. A.; Shi, X.; Xie, F.; Zuo, C.; Konietzko, U.; Shi, K.; Rominger, A.; Xiao, J.; Huang, Q.; et al. Relationship Between Reactive Astrocytes, by [(18)F]SMBT-1 Imaging, with Amyloid-Beta, Tau, Glucose Metabolism, and TSPO in Mouse Models of Alzheimer's Disease. *Mol. Neurobiol* **2024**, DOI: 10.1007/s12035-024-04106-7. From NLM.

https://doi.org/10.1021/acschemneuro.4c00067
ACS Chem. Neurosci. 2024, 15, 2112−2120